Observations of long-period structures associated with charge ordering in $Bi_{0.2}Ca_{0.8}MnO_3$

Y. Murakami and D. Shindo
Institute for Advanced Materials Processing, Tohoku University, Katahira, Sendai 980-77, Japan

H. Chiba, M. Kikuchi, and Y. Syono
Institute for Materials Research, Tohoku University, Katahira, Sendai 980-77, Japan
(Received 27 December 1996)

Long-period structures with 32- and 36-fold periodicity to the original unit lattice distance were observed in a perovskite manganese oxide $Bi_{0.2}Ca_{0.8}MnO_3$ at around 130 K, in addition to the one with fourfold periodicity. Quantitative electron diffraction profiles were measured for the long-period structure, where the intensity of superlattice reflections was observed to increase with increasing scattering angle due to static strain. This result gave a reasonable explanation for occurrence of the charge ordering of Mn^{3+} and Mn^{4+} ions, which was responsible for the creation of the long-period structures in $Bi_{0.2}Ca_{0.8}MnO_3$. [S0163-1829(97)01922-X]

I. INTRODUCTION

Perovskite manganese oxides, such as $La_{1-x}Ca_xMnO_3$, have attracted the considerable attention of many researchers because of the colossal magnetoresistance,[1–3] etc. Charge ordering of Mn^{3+} and Mn^{4+} ions, which is observed in oxides with a specific composition, is one of the attractive phenomena. The two types of manganese ions are randomly distributed in a specimen (at the manganese site of the perovskite structure) at around room temperature. If the specimen is cooled down, however, those ions are believed to be regularly sited. Wollan and Koehler[4] discussed the charge-ordered structures in $La_{1-x}Ca_xMnO_3$ by considering the magnetic structures determined by a neutron-diffraction method. It was recently reported that the charge ordering in perovskite transition metal oxides was observable as apparent superlattice reflections by conventional electron-diffraction methods.[5–8] However, a detailed investigation seems to be still necessary for the charge ordering from the viewpoint of diffraction theory; e.g., the associated superlattice reflections should be extremely weak as far as consideration of the scattering amplitudes of the manganese ions.

$Bi_{1-x}Ca_xMnO_3$ ($x \geqslant 0.8$) was recently studied, both electric and magnetic properties in detail.[9] Considerable magnetoresistance was observed in the oxides, and the occurrence of charge ordering was predicted. More recently, both magnetic and structural transformations in $Bi_{1-x}Ca_xMnO_3$ ($0.74 \leqslant x \leqslant 0.82$) were investigated by means of a neutron-diffraction method, in which a long-period structure with four-fold periodicity to the original orthorhombic lattice distance was observed below room temperature.[10] It was also reported that the structural transformation temperature (e.g., 210 K for $x=0.82$) did not correspond to the magnetic transformation temperature (e.g., 160 K for $x=0.82$). This point seems to be essential in the perovskite manganese oxides.[6,7,10–13]

The purpose of the present work is to investigate both the structure and morphology of the low-temperature phase in $Bi_{0.2}Ca_{0.8}MnO_3$ in detail and to discuss the charge ordering in this oxide by precise electron microscopic methods.

II. EXPERIMENTAL PROCEDURE

A way to fabricate $Bi_{0.2}Ca_{0.8}MnO_3$ ceramic specimens was described in a previous paper in detail.[9] The oxygen content of the specimen was determined to be 2.98 by the iodine titration method. The temperature dependence of the electric resistance was measured by the conventional four-terminal method. The magnetization vs temperature curve was obtained by using a Quantum Design superconducting quantum interference device (SQUID) magnetometer. The structural transformation was studied by using electron microscopes JEM-2010 and JEM-2000EX, employing cooling specimen holders. The intensity distribution in electron diffraction patterns was quantitatively measured by using imaging plates (Fuji FDL-URV) (Ref. 14) or directly measured from films by using a film scanner (Nikon LS3510AF).

III. RESULTS AND DISCUSSION

Figure 1 shows the temperature dependence of the electric resistance and magnetization in $Bi_{0.2}Ca_{0.8}MnO_3$. A consider-

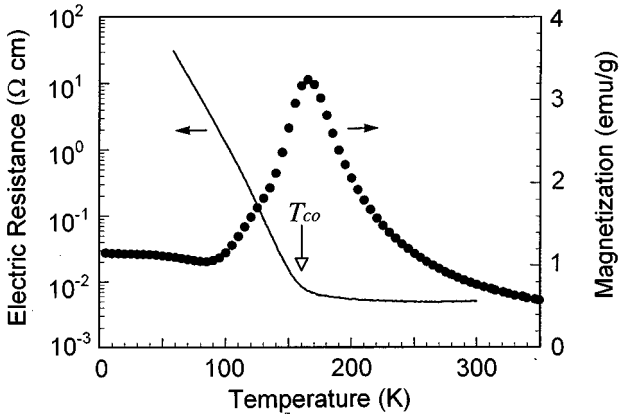

FIG. 1. Temperature dependence of both electric resistance and magnetization in $Bi_{0.2}Ca_{0.8}MnO_3$ measured with cooling the specimen.

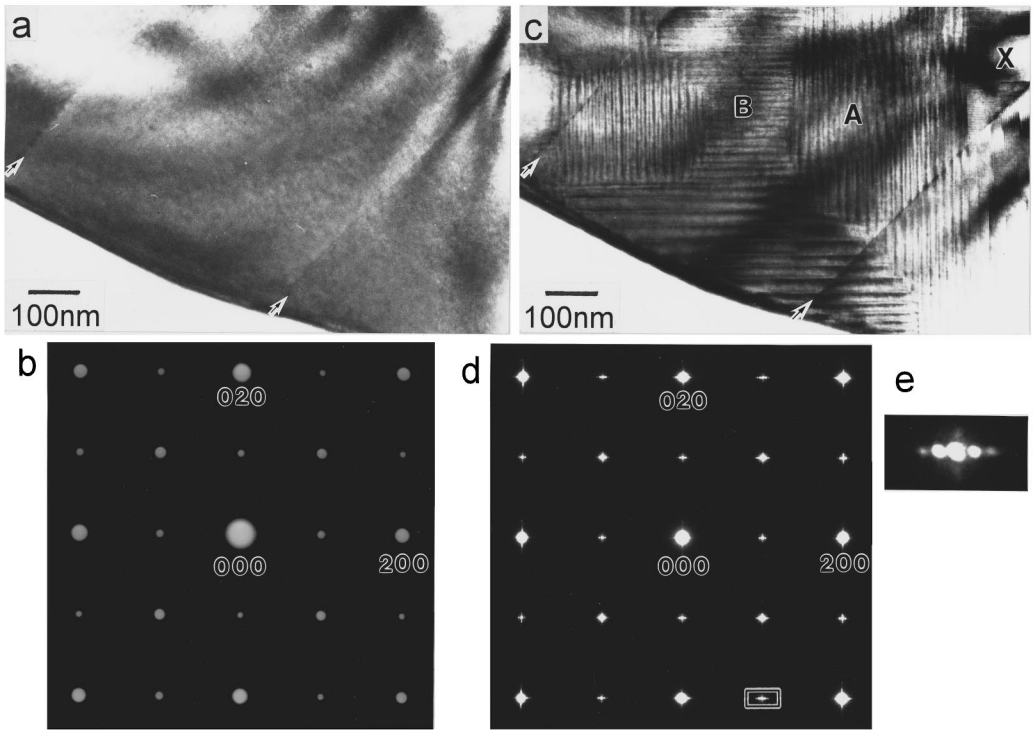

FIG. 2. (a) Typical electron microscopic image and (b) diffraction pattern of $Bi_{0.2}Ca_{0.8}MnO_3$ at room temperature. Both (c) morphological and (d) structural changes were observed by cooling the specimen down to 130 K. The letters *A*, *B*, and *X* in (c) represent domains at 130 K. (e) An enlarged picture for the enclosed area in diffraction pattern of (d). See text for details.

able increase of electric resistance was observed with decreasing temperature below the critical temperature (T_{CO}) at around 160 K. The magnetization curve, which was measured under a magnetic field of 1 T, showed an anomaly at around 160 K, but it was greatly suppressed below T_{CO}.Those results are quite consistent with features of the charge-ordered state suggested by Kuwahara *et al.*[15] Bao *et al.*[10] reported that the magnetic structure in $Bi_{1-x}Ca_xMnO_3$ with a close composition to the present one ($x=0.82$) showed the *C*-type antiferromagnetic structure below the charge ordering temperature. If we consider those results, the charge ordering of Mn^{3+} and Mn^{4+} ions is thought to occur at around $T_{CO}=160$ K and the magnetic structure to transform from paramagnetic to antiferromagnetic below T_{CO}.

Figure 2(a) shows a typical electron microscopic image of $Bi_{0.2}Ca_{0.8}MnO_3$ at room temperature, in which an appreciable fine structure is not visible except for small-angle tilt boundaries marked by arrows. The electron-diffraction pattern in Fig. 2(b), which was taken from the grain surrounded by the small-angle tilt boundaries in Fig. 2(a), could be indexed by taking a *Pbnm* orthorhombic structure with the lattice correspondence of $a\sim\sqrt{2}a_c$, $b\sim\sqrt{2}a_c$ and $c\sim 2a_c$, where a_c represents a lattice parameter of the ideally cubic perovskite structure. When the same specimen was cooled in an electron microscope down to about 130 K (i.e., below T_{CO}), a considerable structural change was observed both in images and diffraction patterns. Two distinct domain structures were observed as shown in Fig. 2(c), i.e., the one with wide-band-like morphology (*A* or *B*) and the other one with narrow-band-like morphology (*X*). The former one consisted of two types of domains *A* and *B*. The bandlike morphology was found to be parallel to either (100) (for domain *A*) or (010) (for domain *B*) plane of the original orthorhombic lattice. Although the bandwidth was slightly different depending on domains, they were typically in the size of 16–20 nm in this type of domain structure. Figure 2(d) shows an electron-diffraction pattern taken from the central grain in Fig. 2(c), in which both the domains *A* and *B* are included. An appreciable change in lattice parameters was not observed for the original orthorhombic lattice by cooling down to 130 K, as far as analyses of electron-diffraction patterns were carried out. However, we recognize existing satellite reflections around Bragg peaks along a^* and b^* axes [i.e., along wave vectors $\mathbf{q}=(1,0,0)$ and $(0,1,0)$ in reciprocal lattice space], which indicates the presence of a long-period structure. The satellite reflections are more clearly seen from Fig. 2(e), which is an enlarged picture of the area enclosed by white lines in Fig. 2(d). The selected-area diffraction method revealed that the satellite reflections along the a^* and b^* axes originated from domains *A* and *B* in Fig. 2(c), respectively. The periodicity of the structure was determined by analyzing the satellite reflections along the a^* axis. They were found to be present at around 1/32 positions between the fundamental reflections (e.g., 1/32, 1/32 0 and 2/32 2/32 0, etc.), which represents periodicity of about 17.0 nm in real space (i.e., 32-fold periodicity to the unit lattice distance of the original orthorhombic lattice), although they were only visible around the fundamental reflections. This value reasonably corresponded to the bandwidth observed for domain *A* in Fig. 2(c). Thus the structural phase transformation in $Bi_{0.2}Ca_{0.8}MnO_3$, which produced the domain structure with wide-band-like morphology, was characterized to be the formation of a long-period structure with the 32-fold

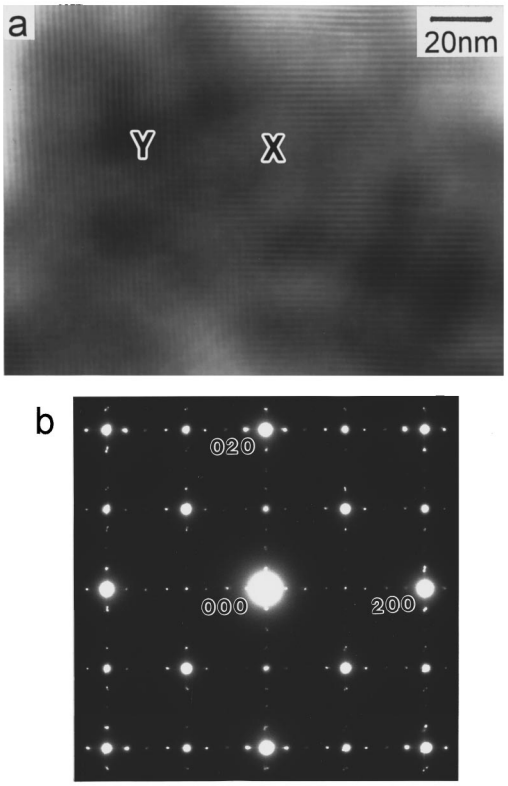

FIG. 3. (a) Typical electron microscopic image and (b) diffraction pattern of $Bi_{0.2}Ca_{0.8}MnO_3$ at 130 K. Two domains of *X* and *Y* were present. See text for details.

periodicity to the original unit lattice distance. Another long-period structure, which had a periodicity of about 36-fold to the original unit lattice distance, was observed in other domains. However, the structure with the 32-fold periodicity was more frequently observed compared to the one with the 36-fold periodicity. It should be noted that those long-period structures were observed for the first time in $Bi_{1-x}Ca_xMnO_3$ exhibiting the negative magnetoresistance. The other type of domain structure was observed around point *X* in Fig. 2(c). The bandwidth in domain *X* was measured to be 2.1 nm, which was much smaller than the value in domain *A* (17.0 nm). This type of domain structure (with narrow-band-like morphology) is also shown in Fig. 3(a), together with the corresponding diffraction pattern in Fig. 3(b), which was taken at around 130 K. Superlattice reflections existed at 1/4 positions between the fundamental reflections along the a^* and b^* axes (e.g., 1/4 1/4 0 and 2/4 2/4 0, etc.), which represent a long-period structure with four-fold periodicity to the original unit lattice distance. Those superlattice reflections were found to be present at the commensurate positions (1/4 positions) in reciprocal lattice space by a quantitative analysis with imaging plates. Two domains *X* and *Y* [i.e., parallel to (010) and (100), respectively] were also present in this type of domain structure, as seen from Fig. 3(a). Similar superlattice reflections at around 1/4 positions were also observed in $Bi_{0.18}Ca_{0.82}MnO_3$ by Bao *et al.*,[10] although they were present at incommensurate positions in reciprocal lattice space. If we observe the diffraction pattern in Fig. 3(b) more in detail, we notice that the superlattice reflections are somewhat splitting. This effect is possibly due to a small orientational deviation between existing domains. Although two types of domain structures (with wide and narrow bands) were observed in $Bi_{0.2}Ca_{0.8}MnO_3$, they are thought to be produced by a similar mechanism because of crystallographic similarities as follows. Both types of domain structures consisted of two domains, each of which was parallel to the (100) and (010) planes of the original orthorhombic lattice, respectively. The superlattice reflections were observed along the a^* and b^* axes in both cases. Only one difference lied in periodicity of the long-period structures.

The two types of domain structures (with wide and narrow bands) disappeared by heating the specimen to room temperature, but they were again observed by a subsequent cooling experiment. However, the same configuration as the previous one was not reproduced; i.e., the two types of domain structures were arranged in a different manner in the second cooling experiment. This point suggests that the formation of the two types of domain structures (with wide and narrow bands) is not attributed to a compositional inequality of the specimen. The domain structure with wide-band-like morphology was more frequently observed compared to the one with narrow-band-like morphology.

Domain structures in perovskite oxides have been observed by some researchers to date. Wang and Zhang[16] observed a domain structure in $La_{1-x}Sr_xCoO_3$, together with superlattice reflections at around room temperature. By means of a high-resolution electron microscopic method, they concluded that the ordering of cations (i.e., La^{3+} and Sr^{2+}) along the $\langle 001\rangle_C$ axis was responsible for creation of the domain structure and the superlattice reflections, where *C* represents indices for the ideally cubic perovskite structure. Such a cations ordering does not seem to be valid for the present case, since the domain structures appeared at around 130 K, where the diffusion mechanism was depressed. Chen and Cheong[8] showed a characteristic domain structure in $La_{1-x}Ca_xMnO_3$ at 95 K, in which platelike morphology was observed parallel to $\{001\}_C$ planes of the cubic perovskite structure, while in the present case parallel to $\{011\}_C$. They reported that the domain structure was accompanied by apparent superlattice reflections, which were interpreted to be due to the charge ordering of Mn^{3+} and Mn^{4+} ions. However, a description was not given for a feature of the relatively strong superlattice reflections in the obtained diffraction pattern. In fact, if the contribution of the charge ordering to diffraction patterns is considered on the basis of structure factor calculations, the intensity of the superlattice reflections should be extremely weak because of a slight difference of scattering amplitudes between Mn^{3+} and Mn^{4+} ions. Both the domain structures and the superlattice reflections observed in the present work are also expected to be due to the charge ordering of Mn^{3+} and Mn^{4+} ions, as expected from the results in Fig. 1. Although the charge ordering will be difficult to be detected as far as the consideration of scattering amplitudes, it is expected to be observable as presence of static strain associated with the ordering. The appearance of the static strain associated with charge ordering is quite reasonable, since the Mn^{3+} ions are accompanied by intrinsic strain due to the Jahn-Teller effect. As is well known, the presence of static strain produces a characteristic intensity distribution in diffraction patterns, where the asso-

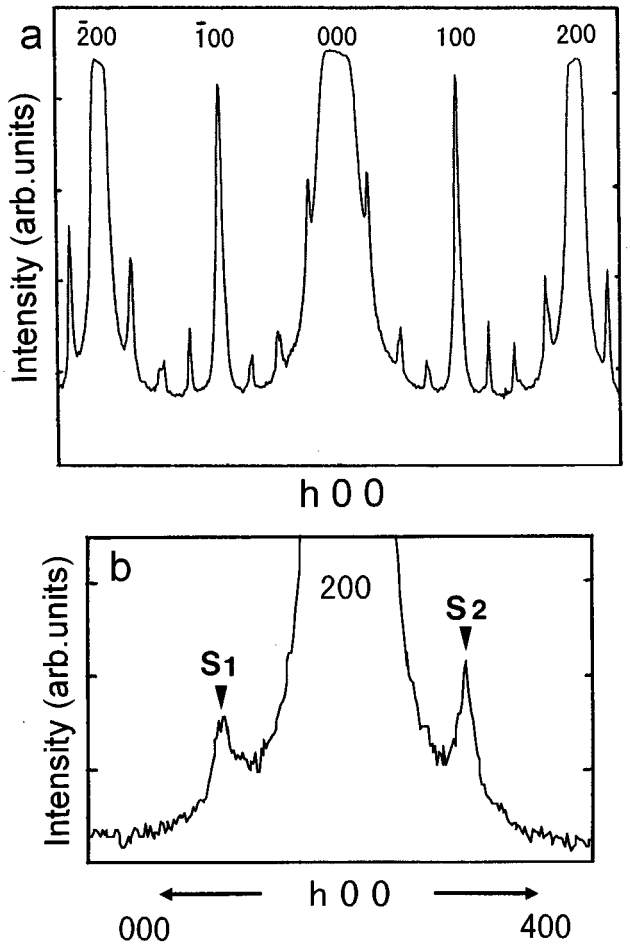

FIG. 4. (a) Intensity profiles along the a^* axis for the superlattice reflections in Fig. 3(b). (b) Intensity distribution around the 200 Bragg reflection precisely measured by an imaging plate. See text for details.

ciated superlattice reflections or diffuse scattering show the intensity maximum at a certain position apart from the origin in reciprocal lattice space.[17] Thus the diffraction profiles tend to increase with increasing scattering angle. Figure 4(a) shows diffraction profiles along the a^* axis, which were measured from the diffraction pattern in Fig. 3(b) (i.e., taken from the domain structure with narrow bands) by using a film scanner. The presence of superlattice reflections at the 1/4 positions is clear. The intensity of the superlattice reflections was observed to increase with increasing scattering angle, which is consistent with the case in the presence of static strain. This effect was more precisely investigated by using an imaging plate, where two specific superlattice reflections beside the 200 Bragg peak were critically measured. The superlattice reflections were shown to be really asymmetric on the intensity as shown in Fig. 4(b), where the one in the higher scattering angle (S_2) was stronger than that in the lower angle (S_1). The dynamical theory of electron diffraction may be necessary to be taken into consideration, since the original intensity distribution (i.e., kinematical intensity distribution) is often modulated by this effect. However, in the present case, the dynamical diffraction effect seems to be small, especially for the superlattice reflections, and the original intensity distribution of the superlattice reflections is thought to be well reflected in the obtained electron-diffraction patterns, because of the following reasons. First, the electron-diffraction patterns were obtained from quite thin regions of the specimen in the present experiment. The dynamical diffraction effect is generally small, if the observed region is quite thin, and the original intensity distribution tends to be well reflected in electron-diffraction patterns without appreciable modulation. Second, the intensity of the present superlattice reflections is much weaker compared to that of the fundamental reflection. The dynamical diffraction effect tends to give only a slight intensity modulation to such weak superlattice reflections, while a significant intensity modulation to the strong reflections. In the former case, a slight modulation occurs so gradually in the reciprocal lattice space.[18,19] Thus the asymmetrization on the intensity between the two weak superlattice reflections beside the 200 Bragg peak [Fig. 4(b)] is thought to originate from the static strain rather than the modulation due to the dynamical diffraction effect. Third, intensity profiles like Fig. 4(a), in which many superlattice reflections were present along the a^* axis, were measured for a few regions with different thicknesses in the specimen. It was confirmed that the intensity of superlattice reflections increased with increasing scattering angle in each region. If we consider those points, the observed intensity distribution of the superlattice reflections (i.e., the intensity increases with increasing scattering angle) can be interpreted as originating from the static strain. However, if we discuss the magnitude of the static strain from the obtained electron-diffraction pattern accurately, a quantitative calculation of the dynamical diffraction effect is necessary based on a precise measurement of the specimen thickness. A similar result to the present one was reported in a neutron-diffraction study for $La_{0.5}Sr_{1.5}MnO_4$ by Sternlieb *et al.*,[13] where the dynamical diffraction effect due to multiple scattering could be negligible. The occurrence of the charge ordering of Mn^{3+} and Mn^{4+} ions in $Bi_{0.2}Ca_{0.8}MnO_3$ was thus rationalized by the detection of static strain associated with this mechanism. The observed long-period structures are thought to be created as a result of the charge ordering. The strain energy due to the charge ordering is interpreted to be minimized by the combination of two domains [e.g., *A* and *B* in Fig. 2(c)] in a macroscopic scale.

Then a question arises as to why the two types of long-period structures (i.e., the ones accompanied by wide- and narrow-band-like morphologies) appear associated with the charge ordering. The electron microscopic observations revealed that domains with the narrow-band-like morphology constantly show the four-fold periodicity to the original unit lattice distance, while the observed periodicity was somewhat different depending on domains in the case of wide-band-like morphology (e.g., 32-fold or 36-fold). It is expected that the four-fold periodicity is the favorable structure associated with the charge ordering in $Bi_{0.2}Ca_{0.8}MnO_3$, since this periodicity is realized in every domain exhibiting the narrow-band-like morphology. However, it is thought that this ordered structure cannot be realized in the entire volume of the specimen because of a compositional restriction, where the content of Mn^{3+} ions is much larger than that of Mn^{4+}. Under this circumstance, the charge ordering may be achieved by taking other long-period structures surrounding the favorable domains with four-fold periodicity. In fact, the

observed periodicity for the wide-band-like morphology corresponds to multiples of the original four-fold one (e.g., 32-fold or 36-fold), which suggests a close relation between the two types of domain structures. A further investigation is now under way on the nature of the long-period structures associated with the charge ordering.

ACKNOWLEDGMENTS

The authors are grateful to S. Ito for useful discussions. This work was supported by a Grant-in-Aid for Scientific Research from the Ministry of Education, Science and Culture in Japan.

[1] R. von Helmolt, J. Wecker, B. Holzapfel, M. Schultz, and K. Samwer, Phys. Rev. Lett. **71**, 2331 (1993).
[2] S. Jin, T. H. Tiefel, M. McCormack, R. A. Fastnacht, R. Ramesh, and L. H. Chen, Science **264**, 413 (1994).
[3] Y. Tomioka, A. Asamitsu, Y. Moritomo, and Y. Tokura, J. Phys. Soc. Jpn. **64**, 3626 (1995).
[4] E. O. Wollan and W. C. Koehler, Phys. Rev. **100**, 545 (1955).
[5] C. H. Chen, S.-W. Cheong, and A. S. Cooper, Phys. Rev. Lett. **71**, 2461 (1993).
[6] Y. Moritomo, Y. Tomioka, A. Asamitsu, Y. Tokura, and Y. Matsui, Phys. Rev. B **51**, 3297 (1995).
[7] A. P. Pamirez, P. Schiffer, S.-W. Cheong, C. H. Chen, W. Bao, T. T. M. Palstra, P. L. Gammel, D. J. Bishop, and B. Zegarski, Phys. Rev. Lett. **76**, 3188 (1996).
[8] C. H. Chen and S.-W. Cheong, Phys. Rev. Lett. **76**, 4042 (1996).
[9] H. Chiba, M. Kikuchi, K. Kusaba, Y. Muraoka, and Y. Syono, J. Solid State Commun. **99**, 499 (1996).
[10] W. Bao, J. D. Axe, C. H. Chen, and S.-W. Cheong, Phys. Rev. Lett. **73**, 543 (1997).
[11] S.-W. Cheong, H. Y. Hwang, C. H. Chen, B. Batlogg, L. W. Rupp, Jr., and S. A. Carter, Phys. Rev. B **49**, 7088 (1994).
[12] W. Bao, C. H. Chen, S. A. Cater, and S.-W. Cheong, J. Solid State Commun. **98**, 55 (1996).
[13] B. J. Sternlieb, J. P. Hill, U. C. Wildgruber, G. M. Luke, B. Nachumi, Y. Moritomo, and Y. Tokura, Phys. Rev. Lett. **76**, 2169 (1996).
[14] D. Shindo, T. Oku, J. Kudo, and T. Oikawa, Ultramicroscopy **54**, 221 (1994).
[15] H. Kuwahara, Y. Tomioka, A. Asamitsu, Y. Moritomo, and Y. Tokura, Science **270**, 961 (1995).
[16] Z. L. Wang and Jiming Zhang, Phys. Rev. B **54**, 1153 (1996).
[17] J. M. Cowley, *Diffraction Physics* (North-Holland, Amsterdam, 1975).
[18] J. M. Cowley and A. D. Pogany, Acta Crystallogr. A **24**, 109 (1968).
[19] D. Shindo, K. Hiraga, T. Oikawa, and N. Mori, J. Electron Microsc. **39**, 449 (1990).